Research Article

Unravelling the Methylene Blue Adsorption Mechanism on Doped and Nondoped Polyaniline: A Combined Molecular Modeling and Experimental Investigation

Souad Djellali [iD],[1,2] **Amani Touati,**[3] **Abderrahmane Semmeq,**[4] **Maya Kebaili,**[5] **Michael Badawi** [iD],[4] **and Adrián Bonilla-Petriciolet** [iD][6]

[1]*Laboratoire de Physico-Chimie des Hauts Polymères (LPCHP), Faculty of Technology, University Ferhat Abbas-Setif 1, Setif 19000, Algeria*
[2]*Department of Chemistry, Faculty of Sciences, University Ferhat Abbas-Setif 1, Setif, Algeria*
[3]*Department of Matter Sciences, University Mohamed Elbachir Elibrahimi, Bordj Bouarreridj, Algeria*
[4]*Université de Lorraine and CNRS, LPCT UMR 7019, F-54000 Nancy, France*
[5]*Centre de Recherche En Mécanique, Campus Chaab Erssase, Université Constantine 1, Constantine, Algeria*
[6]*Chemical Engineering Department, Instituto Tecnológico de Aguascalientes, Aguascalientes 20256, Mexico*

Correspondence should be addressed to Souad Djellali; djellali.souad@yahoo.fr and Adrián Bonilla-Petriciolet; adrian.bp@aguascalientes.tecnm.mx

A multiscale investigation including computational chemistry calculations and experimental studies was performed to elucidate and understand the methylene blue (MB) adsorption on polyaniline (PANI) from an aqueous solution. Static DFT and DFT-based ab initio molecular dynamics were used to characterize the intermolecular interactions of this dye molecule with nondoped and doped PANI. Experimental adsorption studies at different operating conditions were performed to complement the mechanism analysis of this adsorption system. Infrared spectroscopy studies and ab initio calculations showed the important role of π-π stacking and van der Waals interactions for the dye adsorption on PANI. Experimental results of MB adsorption on the PANI surface indicated that alkaline conditions were more favorable than acidic conditions where the MB adsorption capacity ranged from 9.91 mg/g at pH 1.8 to 23.16 mg/g at pH 10.9. Equilibrium adsorption studies with nondoped PANI revealed a fast removal of the dye molecules where the equilibrium adsorption was reached after 45 minutes. The kinetic parameters were calculated with the pseudo-second and pseudo-first order models, while the adsorption mechanism was analyzed using the intraparticle diffusion, Boyd, and Elovich models. Dye adsorption equilibrium was studied at pH 8 and 30 °C where Temkin, Freundlich, Langmuir, and Dubinin-Radushkevich (D-R) isotherm models as well as a statistical physics monolayer model were employed in data analysis. The saturation dye adsorption capacity was 40.2 mg/g where an inclined adsorption orientation of dye molecules on the PANI surface could be expected with an adsorption energy of 14.0 kJ/mol. This interaction energy clearly indicated that only physical interactions were involved in the MB dye adsorption mechanism, which was also confirmed by the calculations with the D-R isotherm model. These theoretical and experimental results are important to understand the dye adsorption properties of conductive polymers and to consolidate their application in the synthesis of new adsorbents and composites for water treatment.

1. Introduction

Polymers with micro- and nano-structures are relevant in several technological applications thanks to their mechanical and chemical properties [1–5]. It was also shown that these materials could be promising for the treatment and purification of polluted water [6–10]. In this context, conductive polymers, their copolymers, and composites have shown an attractive performance in adsorption, electrocoagulation, and photocatalytic processes [11–16]. These polymers can be

synthesized using simple procedures and inexpensive monomers thus obtaining low-cost materials with tailored morphology and surface chemistry [5, 14, 17]. Examples of these compounds are polythiophene, polypyrrole, polyphenylsulfide, polyphenylene, polyacetylene, and polyaniline (PANI) [16, 18].

PANI has been widely studied in adsorption applications [5, 13–15]. This polymer can exist in various forms that differ in color, stability, electrical conductivity, and other physicochemical properties [19]. It can be easily obtained *via* the chemical oxidation of aniline with acidic aqueous solutions, thus generating the conducting doped form named "Emeraldine Salt" (PANI-ES) [20]. The latter form can be converted by a simple base treatment into the electrical insulator nondoped form termed "Emeraldine Base" (PANI-EB) [17].

Several studies have underlined the potentiality of PANI and its related materials as effective adsorbents for inorganic and organic pollutants including dye molecules [13–15, 21–26]. Raw PANI, cross-linked PANI, PANI nanotubes, PANI nanofibers, and PANI composites obtained from chitosan, lignocellulose, starch, graphene, clays, and zeolites have been employed in water decolorization to remove a variety of dye molecules, e.g., reactive black 5, congo red, acid green 25, rhodamine *B*, methylene blue (MB), orange *G*, basic blue 41, acid green 25, acid violet 90, and acid yellow 194 [5, 13, 16, 27–30]. Dye adsorption using PANI-based materials has proved to be more effective than other treatment methods, which have the disadvantages of high operating costs and low removal efficacy [31, 32]. Different studies have concluded that PANI and its composites can exhibit fast dye adsorption and high removal efficiency compared to other conventional adsorbents. This is mainly owed to their surface functionalities, morphology, and textural parameters [33]. Overall, the dye adsorption capacities displayed by PANI-based adsorbents can range from 10 to 480 mg/g at 25–30 °C and pH 2–10 [5, 13, 26, 28]. For instance, Ayad and El-Nasr [13] employed PANI nanotubes to remove cationic dyes from aqueous solutions. Chowdhury et al. [26] found that an anionic specie can be efficiently removed by the acid-doped PANI, while a cationic dye was preferentially removed by the nondoped PANI. Bhaumik et al. [28] reported the efficient removal of an anionic dye by adsorption onto interconnected polypyrrole-PANI nanofibers.

Although different studies on dye adsorption on PANI adsorbents have been published, their adsorption mechanisms have not been systematically analyzed and explained. Adsorption properties of PANI-based materials have been partially ascribed to amine and imine active groups contained in the polymer backbone. In fact, it has been suggested that the removal mechanisms of dye molecules with these adsorbents could involve electrostatic interactions, hydrophilic or hydrophobic forces, and conjugated π-π electrons interactions [5, 16, 34]. However, no theoretical or experimental evidence has reliably backed these claims about the dye adsorption mechanisms and the possible adsorbent-adsorbate interactions.

From a theoretical perspective, computational chemistry calculations [35] and molecular simulations [36] are reliable tools to understand and explain the intermolecular interactions involved in the dye adsorption mechanism with PANI-based adsorbents. But, a limited number of studies on DFT-based mechanistic analysis for dye—PANI systems have been reported in the literature [35, 37]. Specifically, Li et al. [35] performed DFT-D3 calculations to characterize the mechanism of methyl orange dye adsorption on PANI from an aqueous solution. They concluded that hydrogen bond and van der Waals forces were responsible for the interactions of methyl orange adsorption on the PANI surface. The interaction energy between methyl orange molecule and PANI was also calculated using DFT to complement the analysis of dye adsorption on a magnetic PANI-silica nanocomposite [37]. The latter study also confirmed the presence of hydrogen bonding for the adsorption of this dye molecule. It is convenient to highlight that the dye separation performance of PANI adsorbents is highly pH-dependent [5, 16, 38]. However, several papers have reported the adsorption of dye molecules on PANI-based materials at limited operating conditions (i.e., pH 6–7) [5, 16]. The literature review indicates that the pH effect on the molecular structures of PANI and the corresponding analysis of adsorption mechanisms for other dye molecules have not been fully explained and understood. Computational chemistry studies are indeed necessary to resolve this gap and to enhance and consolidate the understanding and application of conductive polymers in the preparation of effective materials for water purification.

In the present work, a multiscale approach with computational chemistry calculations, kinetic-isotherm modeling, and experimental studies has been realized to elucidate the MB-PANI interactions, describe the electron transfer between adsorbent and adsorbate, and rationalize several aspects of this adsorption system. The novelty of this study was to provide a detailed explanation of the chemical changes occurring in the molecular structure of MB dye and their effect on the adsorption using PANI in acidic, neutral, and alkaline solutions. These findings are fundamental to understanding the surface properties of PANI thus allowing it to optimize its application to prepare composite materials for water treatment. This dye is mostly used for coloring textiles and paper but is primarily regarded as a toxic pollutant in wastewater treatment because it can generate several harmful effects on the human body after intoxication or acute exposure [39]. Therefore, MB was selected as the model dye molecule for the present study. Experimental studies were also done to validate the theoretical findings thus analyzing the MB removal with PANI at various operating conditions (i.e., contact time, initial dye concentration, pH).

2. Materials and Methods

2.1. Molecular Modeling of MB Adsorption on PANI. The adsorption of MB on PANI-EB and PANI-ES was investigated using static DFT and ab initio molecular dynamics (AIMD) within the GGA and PBE methods [40]. DFT computations were performed using Gaussian code (version 09) [41] and employing the implicit solvation where the

effect of the solution was modeled with the C-PCM model (SCCS) [42, 43]. However, due to the high computational cost, AIMD calculations were performed in CP2K [44] and were limited to the gas phase with no periodic boundary conditions applied.

The structure model of PANI-ES and PNI-EB consisted of six benzenoid rings and two quinoid rings (Figure 1). The optimization of PANI molecules was performed using DFT via PBE with a double zeta quality basis-set augmented with polarization functions (DZVP). This level of theory was able to reproduce structural parameters that were in excellent agreement with previous theoretical computations [45]. Ab initio molecular dynamics runs of 100 ps were performed in the case of MB@PANI systems to describe the adsorption modes of MB; then, static optimizations were conducted. AIMD calculations were conducted in the CP2K code within the DFT and the GGA-PBE method. DFT-D2 dispersion correction of Grimme [46] was added to account for non-covalent interactions. The core electrons were treated with the Goedecker, Teter, and Hutter (GTH) Norm-Conserving pseudopotentials [47], while the valence electrons were expanded as double zeta Gaussian functions with polarization (DZVP) [48] within the Gaussian Plane Wave scheme (GPW) [49].

An energy cut-off of 300 Ry was chosen. The canonical ensemble was generated using the GLE thermostat [50] at 300 K, and the trajectories were propagated for 100 ps, including a 15–20 ps equilibration step with a 0.5 fs integration time step. The parameters for the thermostat were obtained from [51]. Subsequently, 0 K DFT calculations were conducted in Gaussian 09D code allowing to model statically the solvation effect as well as computing the IR spectra.

Adsorption energies (E_{ads}) were calculated at 0 and 300 K, according to

$$E_{ads} = E_{MB@PANI} - E_{MB} - E_{PANI}. \quad (1)$$

Energies from AIMD calculations (300 K) were extracted by taking the average of the total energies over the produced trajectory (with the equilibration part omitted) for MB, PANI, and MB/PANI systems.

2.2. Experimental Studies of MB Adsorption on PANI. The chemical synthesis of PANI was performed following the procedure reported by Stejskal and Gilbert [52] using ammonium persulfate $((NH_4)_2S_2O_8)$ as oxidant and hydrochloric acid (1 M HCl) as a dopant. Analytical grade chemicals were used and aniline was bidistilled and stored in darkness at 2 °C prior to its use. The reaction was conducted in a three-necked round-bottom flask immersed in an ice bath (< 4 °C) with a molar ratio oxidant/aniline of 1.5. These experimental conditions limited the secondary reactions and led to a product with a high yield. To complete the polymerization, the mixture was stirred for 4 h, and the dark green precipitate was washed with water, acetone, and 0.1 M HCl and dried at 50 °C. The structural characteristics of synthesized PANI were analyzed with FTIR spectroscopy, UV-Vis
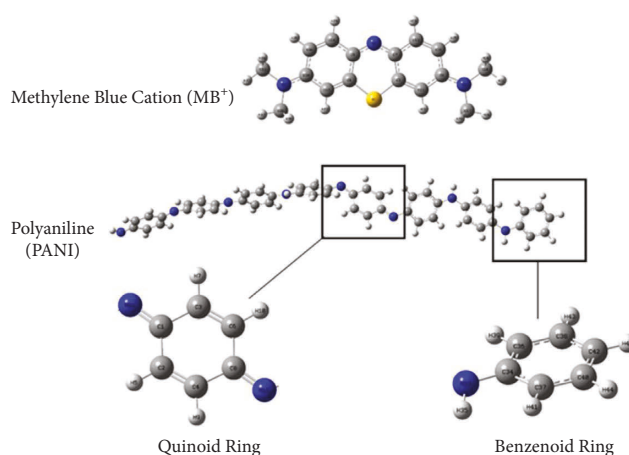

FIGURE 1: Structure representation of MB and quinoid and benzenoid rings of PANI. Nomenclature: carbon is indicated in grey, nitrogen in blue, hydrogen in white, and sulfur in yellow.

spectroscopy, and X-ray diffraction (XRD). These tests were performed, respectively, on a Perkin-Elmer spectrometer in the range 4000–400 cm^{-1}, a Shimadzu UV-Visible spectrophotometer UV1201 in the range 190–1100 nm, and an X''Pert3 Powder diffractometer in the range 2°–60° using CuKα radiation ($\lambda = 1.54$ Å) from $2\theta = 10°$ to 70°, at a scan rate of 0.02/s. Peak crystalline areas were determined with the X'pert HighScore software. The surface morphology of PANI powders was observed at room temperature by scanning electron microscopy (SEM) on a ZEISS GeminiSEM 300 microscope with an accelerating voltage of 2 kVolts. Particles' size of doped and nondoped PANI powders was obtained using the "CILAS 1190" particle size analyzer. Powders were dispersed in water, sonicated for three minutes, and then analyzed under a set of three lasers ensuring the highest level of accuracy and precision.

The synthesized PANI was tested in the MB adsorption from aqueous solutions. A stock solution of 1 g/L of this dye was prepared and used to obtain the working solutions with different concentrations. MB, [7-dimethylamino-3-phenothiazinylidene]-dimethylammonium chloride (Figure 1), is a heterocyclic aromatic compound ($M_w = 319.85$ g/mol; $\lambda_{max} = 661$ nm) and was obtained from Sigma and used as received.

In the experimental adsorption studies, 10 mg of PANI powder was dispersed in the dye solution (50 mL), sonicated to homogenize the mixture and break down the polymer aggregates, and, finally, stirred at room temperature (30 °C) during a specific contact time. MB adsorption on PANI was assessed at different conditions of pH (1.8—11), contact time (5 min—6 h), and initial dye concentration (5—60 mg/L). In all these experiments, centrifugation at 10000 rpm was applied to separate the adsorbent from the aqueous solution and the final dye content was quantified. MB concentrations were determined using a Shimadzu UV-Visible spectrophotometer UV1201 at the wavelength of 661 nm. Batch adsorption experiments were done in triplicate.

MB adsorption capacity (Q, mg/g) and removal efficiency ($R\%$) were determined using the next expressions [53]:

$$Q = \frac{\left(C_0 - C_f\right) \cdot V}{m},$$

$$R\% = \frac{C_0 - C_f}{C_0} \cdot 100, \tag{2}$$

where C_0 and C_f (mg/L) are the initial and final MB concentrations from the adsorption experiment, $m\,(\text{g})$ is the adsorbent mass, and $V(\text{L})$ is the MB solution volume.

Kinetic and equilibrium experimental data of MB adsorption on PANI were correlated with the pseudo-second-order, pseudo-first-order, Langmuir, Freundlich, Temkin, and Dubinin-Radushkevich (D-R) equations as well as a statistical physics monolayer model. Furthermore, the adsorption mechanism was analyzed using the intraparticle diffusion, Boyd, and Elovich models.

Nonlinear regressions were performed for all adsorption models, and the best fit was identified based on the root mean square error (RMSE) and the determination coefficient (R^2).

$$R^2 = 1 - \frac{\sum_{i=1}^{n_{\text{dat}}} \left(Q_{i,\,\exp} - Q_{i,\text{cal}}\right)^2}{\sum_{i=1}^{n_{\text{dat}}} \left(Q_{i,\,\exp} - Q_{i,\exp}\right)^2},$$

$$\text{RMSE} = \sqrt{\frac{\sum_{i=1}^{n_{\text{dat}}} \left(Q_{i,\,\exp} - Q_{i\cdot\text{cal}}\right)^2}{n_{\text{dat}} - n_p}}, \tag{3}$$

where $Q_{i,\text{cal}}$ and $Q_{i,\,\exp}$ are the calculated and experimental MB adsorption capacities, n_p is the number of model parameters, and n_{dat} is the number of experimental points used in the nonlinear regression, respectively.

3. Results and Discussion

3.1. Characterization of PANI. First, infrared spectroscopy was employed to investigate the dye structure and to verify the MB adsorption on the surface of PANI powder at acidic and basic conditions. The experimental FTIR spectrum of this cationic dye, shown in Figure 2, revealed a broad and intense band related to OH groups (3100–3500 cm^{-1}) thus indicating that the MB used in this study was a hydrated compound. The absorption bands corresponding to vibrations of CH groups of the heterocycle and CH$_3$ of the terminal dimethylamino groups were located at 3025, 2950–2920, and 2850 cm^{-1}, respectively [54]. The region of low IR frequencies displayed several bands attributed to bonds of stretching vibrations in the heterocycle, with either strong intensities, like C=C and C=N (1600 cm^{-1}) and C-C and C-N (1545 cm^{-1}), or moderate intensities like C-N (1340 cm^{-1}) and C=S$^+$ (1356 cm^{-1}). Other absorption bands were identified at 1300–600 cm^{-1}, which could be assigned to C-N and C-S-C vibrations of the heterocycle (1142 and 1068 cm^{-1}) to C-H vibrations of different types (890–790, 1184, 1226, 1252, 1394, 1447, and 1490 cm^{-1}), to C-S-C vibrations (615 and 667 cm^{-1}), and to H bonds of the type N$_{\text{het}}$ HO (950 cm^{-1}) [55].
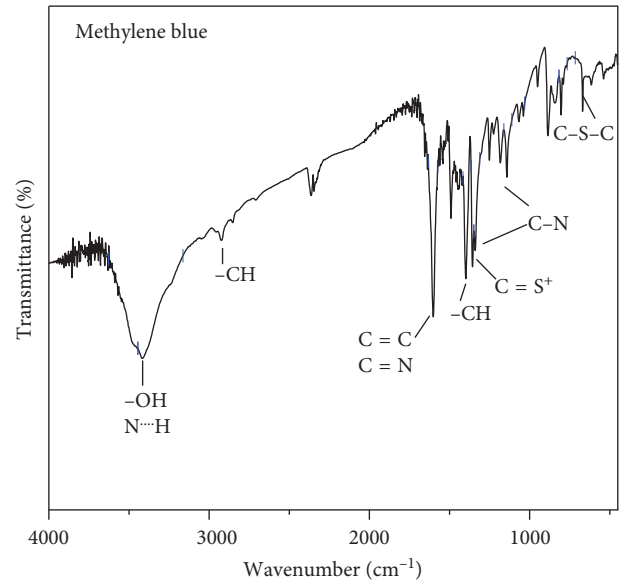

FIGURE 2: Experimental FTIR spectrum of MB.

Figure 3(a) contains the FTIR spectrum of the green-dark powder obtained in this study, which was similar to those found by several authors for HCl-doped PANI [56, 57]. This result indicated that the as-synthesized PANI was in its Emeraldine Salt form (i.e., PANI-ES). FTIR spectrum of PANI-ES pointed out the characteristic vibration bands of C=C groups at 1572 and 1468 cm^{-1} ascribed to the quinoid rings and benzenoid rings of polyaniline, respectively. Other specific vibrations of carbon-nitrogen bonds, mainly C=N and C-N linked to benzene and quinine rings, were identified via the bands in the region of 1400–1240 cm^{-1} [58]. The absorption band located at 1020 cm^{-1} corresponded to the vibrational mode of polaron (–C–NH$^{+\bullet}$) or bipolaron (–C=NH$^{+\bullet}$) structures that were formed in the doping process [57]. Absorption bands between 3000 and 3400 cm^{-1} were attributed to N–H bonds and those between 690 and 800 cm^{-1} were related to the aromatic C–H bond.

FTIR spectrum of PANI-EB sample obtained after the treatment of PANI-ES with an alkaline solution is reported in Figure 3(b). The main characteristic bands of PANI-ES were also identified but with slight shifts to higher frequencies due to the reduction of conjugation in the polymer backbone [58, 59]. Therefore, the absorption bands at 1572, 1468, and 1295 cm^{-1} in the PANI-ES spectrum shifted to 1586, 1499, and 1303 cm^{-1} in the PANI-EB spectrum, respectively, because of the deprotonation process. Consequently, the deprotonation of PANI involving oxidation or reduction reaction, or both, generated the formation of two alternating units containing reduced amino groups (benzenoid ring) and oxidized imine groups (quinoid ring).

The UV-visible spectrum obtained for the synthesized PANI displayed bands characterizing the chromophores of aniline and the p-benzoquinonediimine cation radical and the interaction between them; see Figure 3(c). These bands appeared at ~430 and 870 nm and were attributed to $\pi - \pi^*$
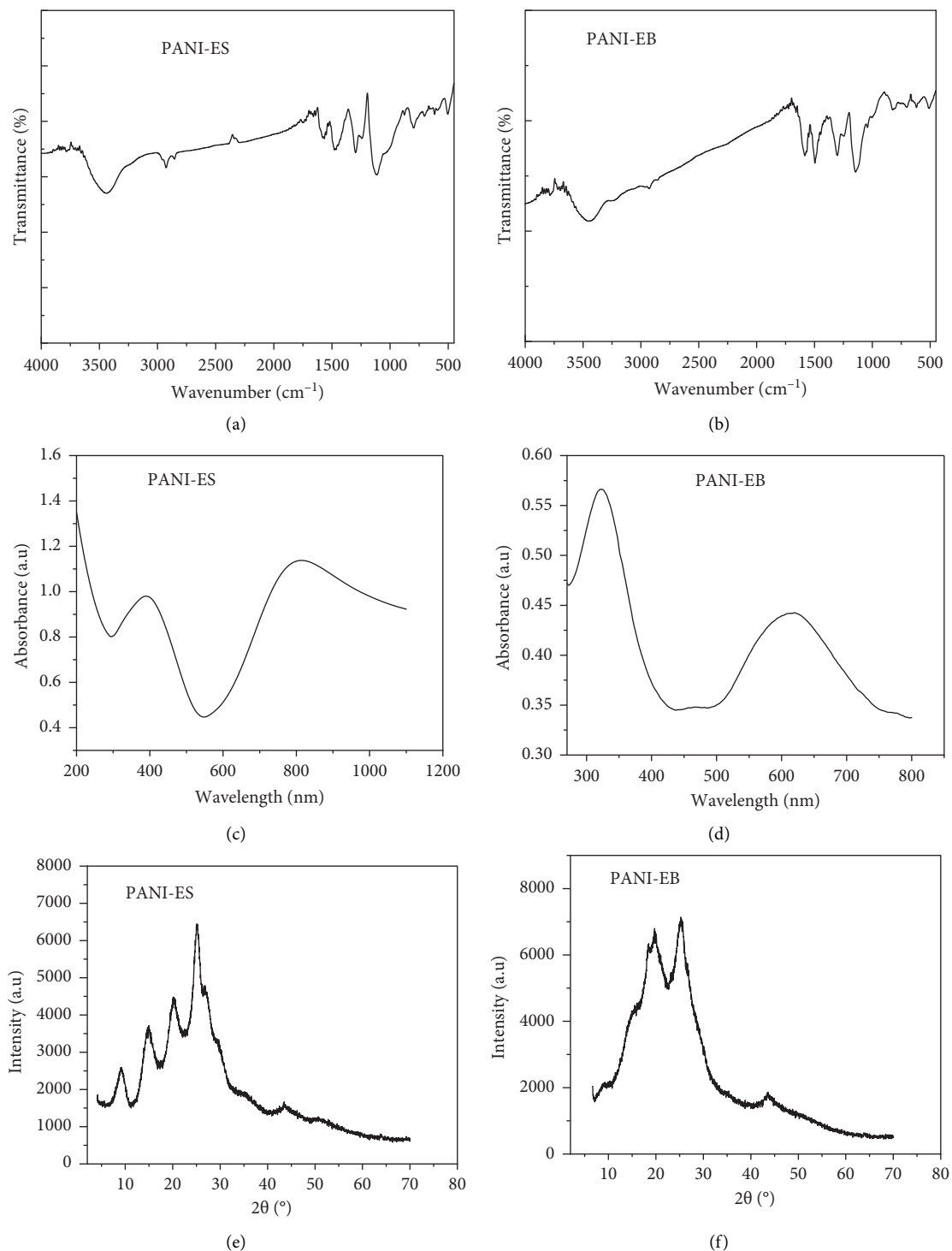
FIGURE 3: (a), (b) FTIR spectra, (c), (d) UV-VIS spectra, and (e), (f) XRD diffractograms of PANI-ES and PANI-EB.

transition in the benzenoid ring, the polaron-π^* transition, and π-polaron transition, respectively [60]. UV-visible absorption results also showed that the PANI-EB backbone structure generated a band at 615 nm, which was ascribed to the benzenoid-quinoid rings charge transfer (Figure 3(d)). Another sharp absorption band at 325 nm was detected and assigned to $\pi - \pi^*$ transitions [61].

XRD patterns of PANI-ES and PANI-EB are presented in Figures 3(e) and 3(f). A semicrystalline pattern was observed for PANI-ES, which exhibited sharp peaks at $2\theta = 9.3°$, $14.8°$, $20.3°$, and $25.2°$, and shoulders at $26.8°$, 29.3. However, the XRD profile of PANI-EB displayed fewer peaks compared to PANI-ES which reflected a loss of crystallinity during the dedoping process. The crystalline

parts of Emeraldine Base displayed several broad reflection peaks at $2\theta = 6.4°$, $9.1°$, $15.7°$, $18.4°$, $19.8°$, and $25.4°$. Larger peaks are believed to be formed by reflections of wider clusters. Similar diffractograms were found in the literature for PANI-ES [62] and PANI-EB [63].

The semicrystalline character of PANI-ES and PANI-EB was confirmed with the values of their degrees of crystallinity (X_c %), which were calculated using the following equation [62]:

$$X_c (\%) = \frac{H_c}{(H_c + H_a)} * 100, \qquad (4)$$

where H_c and H_a are the areas of the crystalline and amorphous profiles. The crystallinity degree value of PANI-ES was 52%, while that of PANI-EB was 19%.

Experimental FTIR spectra obtained after MB adsorption on PANI are displayed in Figure 4. They exhibited the main characteristic absorption bands of both interacting compounds (PANI/MB). However, several bands of these spectra have undergone shifts in their positions, thus supporting the evidence that MB was adsorbed on the PANI surface either in its doped or nondoped states. The main changes in PANI were associated with the amine and imine moieties. The positions of their absorption bands moved from 1572 and 1468 cm^{-1} to 1599 and 1490 cm^{-1} for PANI-ES. However, the absorption band positions of PANI-EB shifted from 1581 and 1495 cm^{-1} to 1618 and 1510 cm^{-1}, respectively. Note that the analysis of these spectra was not straightforward mainly in the fingerprint region due to the close proximity of bond vibrations in MB molecules and in the chain backbone of adsorbents. Similar spectral changes were mentioned in other studies [64, 65], and they were accredited to the participation of different active centers of MB molecules with the adsorbent active sites in donor-acceptor, $\pi - \pi$ stacking, and hydrophobic interactions.

These experimental FTIR spectra were superposed with those computed via DFT for MB@PANI-ES and MB@PANI-EB, as seen in Figure 4. Overall, the comparison of the PANI and MB@PANI systems indicated a good agreement. An analysis of the normal modes belonging to the MB@PANI showed no pronounced vibrational correlation between the adsorbate and adsorbent, which supported the experimental findings about the dispersive nature of MB/PANI interaction.

Finally, SEM images for the analysis of the morphology of doped and nondoped PANI powders are displayed in Figure 5. These images showed irregularly arranged grainy particles, which tended to form small clusters. Such granular morphology has been observed in PANI powders prepared by chemical oxidation [66].

The analysis of PANI powders by laser particle size analyzer (see Figure 5) suggested large particle size distribution and a high polydispersity of particles, which may indicate the occurrence of some particle aggregation. Also, it can be noticed that the average diameter of PANI-ES ($47.8\,\mu m$) was lower than that of PANI-EB ($68.9\,\mu m$) denoting that aggregations of PANI-ES particles were more compact than PANI-EB ones. Therefore, it was concluded that the availability of the ions along PANI-ES backbones

resulted in an increment of the intermolecular forces, significant chain aggregation, and a decrement in the average particle size. Furthermore, the specific surface area measurements for both polymer powders were carried out in previous works where authors reported values of 15 m^2/g for PANI-ES [67, 68] and 29 m^2/g for PANI-EB [68] with N_2 adsorption/desorption isotherms of Type II according to IUPAC classification. PANI can be considered as an adsorbent with low porosity and, consequently, it could be expected that the MB adsorption occurred mainly on the external surface of this polymer.

3.2. MB@PANI Adsorption Dynamics.

The experimental and theoretical IR spectra suggested a $\pi - \pi$ stacking type adsorption of MB on PANI. In this section, a systematic analysis of the MB adsorption on PANI-EB and PANI-ES is provided by describing their respective adsorption intermolecular interactions and energies.

Figure 6 shows the molecular structures of MB-PANI systems obtained from ab initio calculations, while Table 1 reports the energies computed using DFT and AIMD for the MB adsorption on PANI-EB and PANI-ES, as well as their deformation energies. Both methods predicted the adsorption energy of MB on PANI-EB higher than that on PANI-ES, thus indicating a higher adherence of the former to the MB molecules. These results were in full agreement with the experimental MB adsorption studies as will be described below.

The theoretical calculations indicated that the main driving interactions were of dispersive nature where both PANI-EB and PANI-ES interacted with MB mainly through $\pi - \pi$ stacking. While the computed adsorption energy difference was rather low, their adsorption behavior can be explained by the slightly different adsorption modes. On PANI-EB, the adsorption of MB was angled thus allowing a higher adsorption rate per PANI-EB molecule. On the other hand, the MB adsorption on PANI-ES was more likely to occur parallel with the adsorbent surface, thus needing a higher effective area.

The electronic properties of PANI adsorbents were investigated to gain insight into their reactivity and behavior toward this organic adsorbate. In this direction, the frontier orbital energies E_{HOMO} and E_{LUMO} indicated an obvious contrast in the capability to give or accept electrons. It can be noted that PANI-EB had a minimal gap compared to PANI-ES, which can cause it to be more reactive toward MB molecules. The quantum chemical descriptors of the studied MB/PANI-EB and MB/PANI-ES systems are illustrated in Figure 7 and Table 2.

The electronegativity values in Table 2 show that electron flux can occur from the MB toward the PANI surface showing the highest electronegativity. From Figure 7 and Table 2, it was concluded that PANI-EB was more reactive than PANI-ES because of its lesser gap values in gas and solvated states, which could indicate that MB could be adsorbed more easily and quantitatively higher on PANI-EB than PANI-ES. Experimental adsorption results that will be discussed in the next section confirmed these theoretical findings.
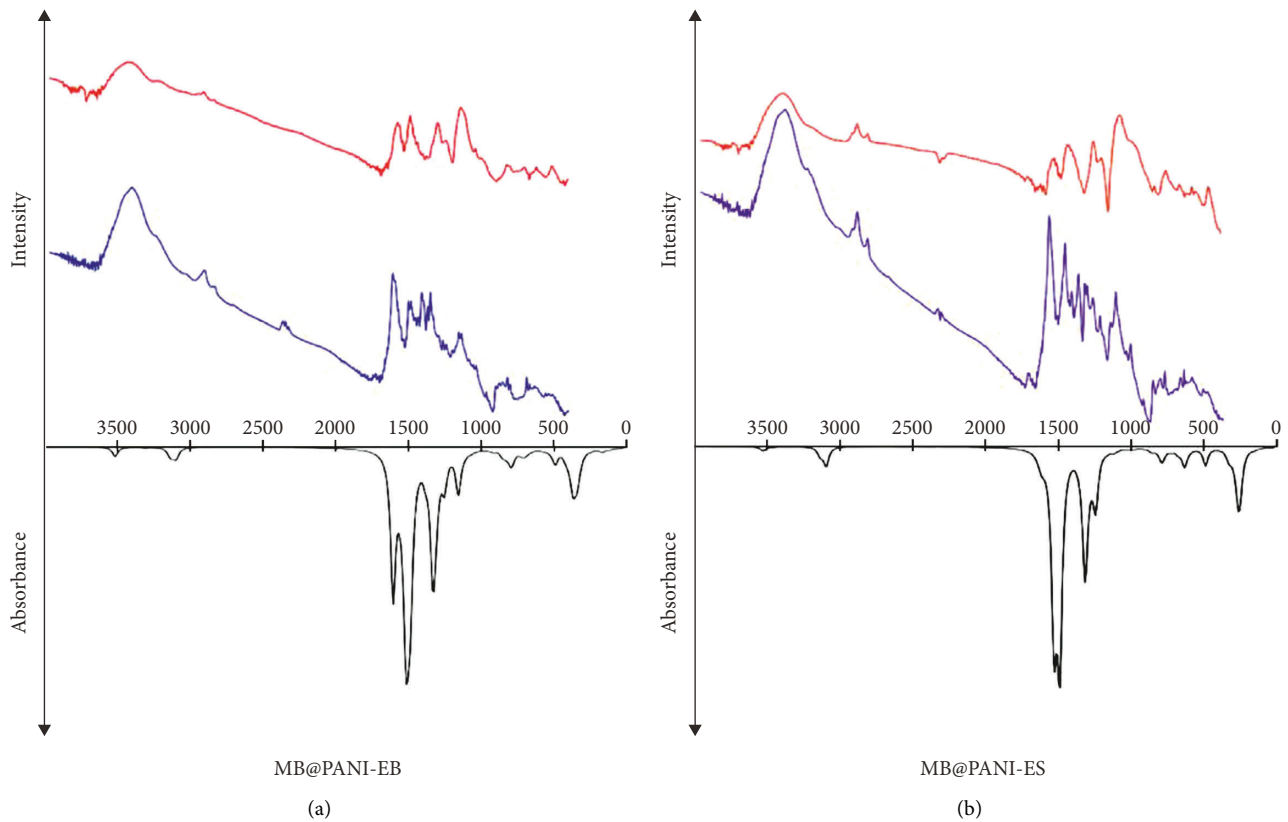
MB@PANI-EB

(a)

MB@PANI-ES

(b)

FIGURE 4: Experimental FTIR spectra of PANI (red) and MB@PANI systems (blue) and their comparison with DFT computed IR spectra (black) of MB@PANI. Samples: (a) PANI-EB (base-treated) and (b) PANI-ES (acid-treated).
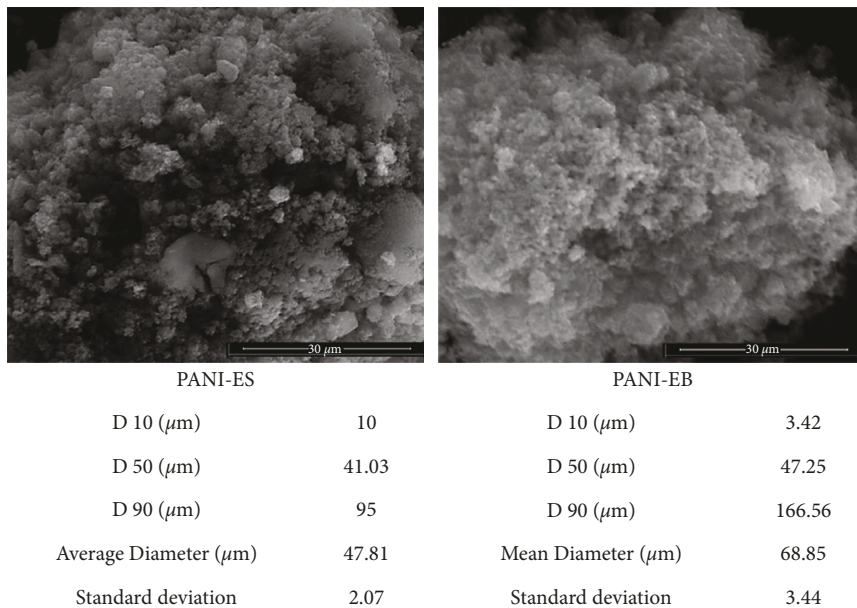

PANI-ES		PANI-EB	
D 10 (μm)	10	D 10 (μm)	3.42
D 50 (μm)	41.03	D 50 (μm)	47.25
D 90 (μm)	95	D 90 (μm)	166.56
Average Diameter (μm)	47.81	Mean Diameter (μm)	68.85
Standard deviation	2.07	Standard deviation	3.44

FIGURE 5: SEM images and particle size parameters of PANI-ES and PANI-EB powders.

3.3. Adsorption of MB on Doped/Undoped PANI

3.3.1. Effect of the pH on PANI Adsorption Capacity.
The effect of solution pH on MB adsorption was experimentally investigated due to its crucial role in dye removal. This parameter can affect the surface charge, the protonation of adsorbent active sites, and the dye speciation distribution. The results of the pH effect on MB adsorption on the PANI surface are shown in Figure 8. Overall, the adsorbed MB quantity increased with the pH solution from acidic
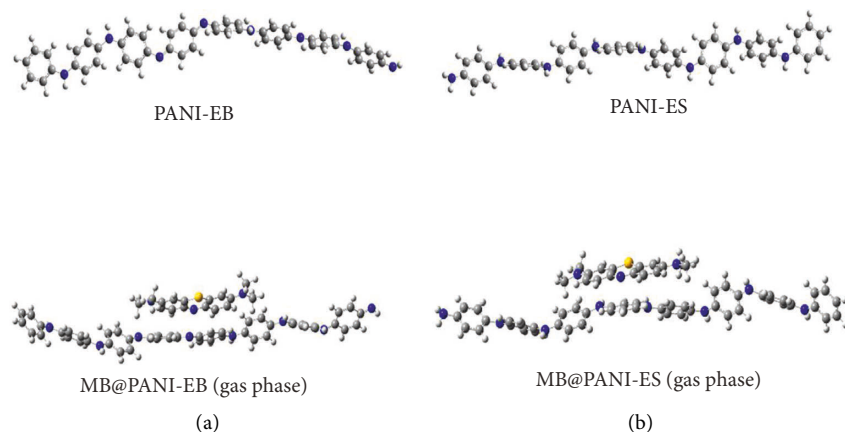
PANI-EB

PANI-ES

MB@PANI-EB (gas phase)

MB@PANI-ES (gas phase)

(a)

(b)

FIGURE 6: Structures of the (a) PANI-EB and (b) PANI-ES before and after the adsorption of MB from ab initio calculations.

Methylene-Blue

Gas Phase

S (1):0.114;N (4):0.083

S (1):0.076;N (2):0.054;0.063;N (3):0.054

In Solvent

S (1):0.124;N (4):0.094

S (1):0.073;N (2):0.054;N (3):0.054

PANI-EB

Gas Phase

N (93):0.076;N (57):0.061

N (91):0.031;N (93):0.024;H (87):0.022;
H (31):0.021;N (22):0.031;N (11):0.023

In Solvent

N (93):0.085;N (57):0.072

N (33):0.028;N (22):0.037;N (91):0.028;
N (11):0.023

PANI-ES

Gas Phase

H (96):0.027;H (80):0.025;C (61):0.026

N (11):0.027;N (94):0.023;N (33):0.023;N (22):0.027
H (20):0.024;H (31):0.023;H (18):0.024;H (7):0.023

In Solvent

C (61):0.027;C (62):0.027;C (66):0.028;C (72):0.026;
C (73):0.028;C (77):0.026;C (79):0.028

N (94):0.027;N (45):0.020;N (33):0.028;N (22):0.033
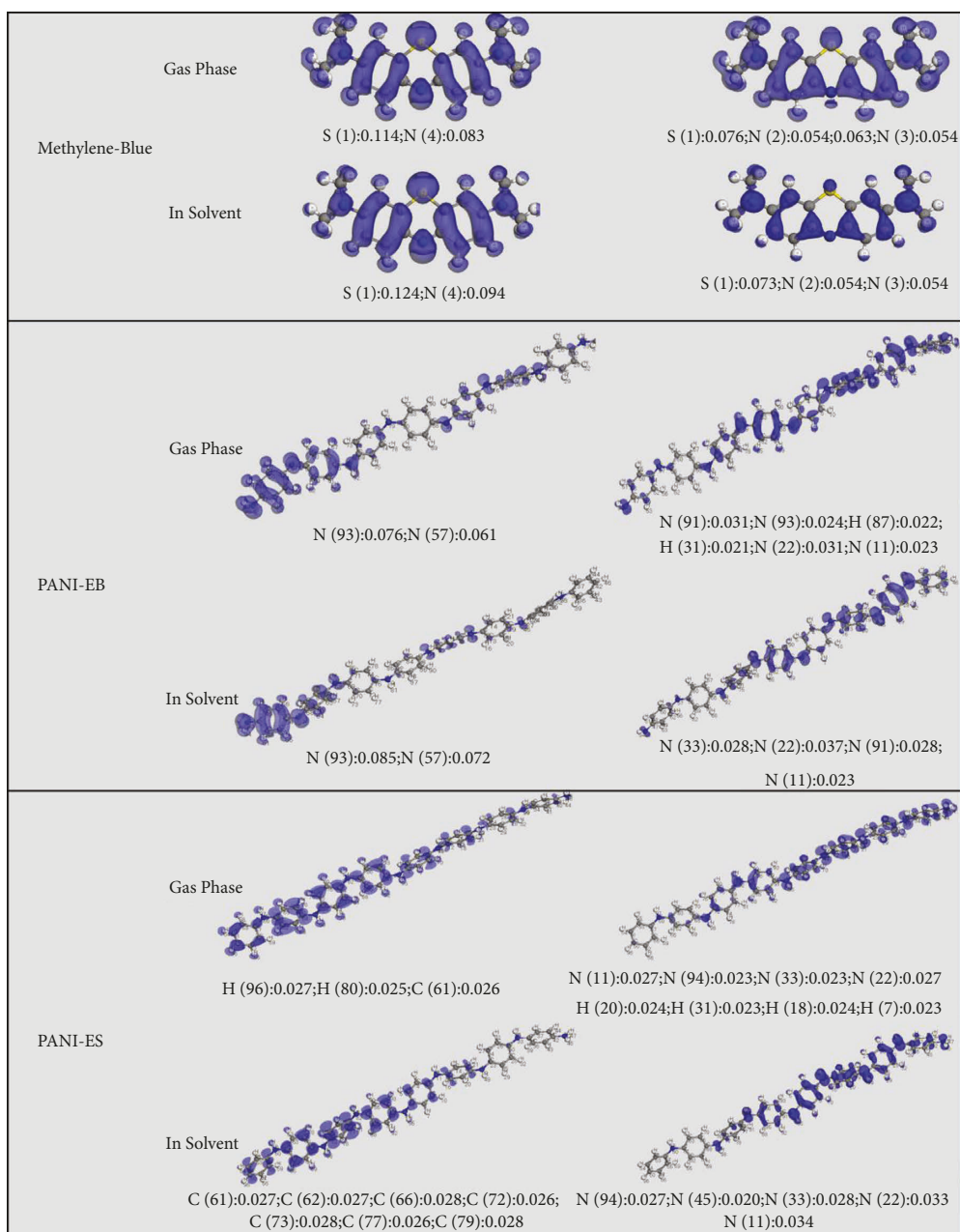N (11):0.034

FIGURE 7: Fukui analysis of MB, PANI-EB, and PANI-ES in the gas phase and liquid phase. The left panel contains values for the nucleophilic term f_k^+ while the second panel gives the electrophilic term f_k^- values of the Fukui function.

TABLE 1: DFT and AIMD adsorption energies (E_{ads}) of MB on PANI-EB and PANI-ES as well as their deformation energies.

| | Adsorption energy (kJ/mol) | | Deformation energy (kJ/mol) |
	DFT	AIMD	
MB/PANI-EB	−9.92	−8.17	−0.54
MB/PANI-ES	−8.45	−7.91	−0.39

TABLE 2: Quantum chemical descriptors of the studied MB/PANI-EB and MB/PANI-ES.

| Parameter | MB | | PANI-EB | | PANI-ES | |
	Gas	Aqueous	Gas	Aqueous	Gas	Aqueous
E_{HOMO} (eV)	−8.125	−5.213	−4.103	−4.274	−3.257	−3.486
E_{LUMO} (eV)	−6.614	−3.803	−3.268	−3.583	−0.826	−1.113
Gap ΔE (eV)	1.511	1.410	0.835	0.691	2.431	2.373
Electronegativity χ	7.369	4.508	3.685	3.928	2.042	2.299
Hardness η	0.755	0.705	0.417	0.345	1.215	1.187
Electrophilicity index ω	35.962	14.413	16.282	22.361	1.716	2.226

conditions (pH~2) to alkaline conditions (pH~11) where the MB adsorption capacity ranged from 9.91 mg/g at pH 1.8 to 23.16 mg/g at pH 10.9. These results were similar to those reported by Chowdhury et al. [26] and Wang et al. [69] which showed a high removal efficiency of PANI for MB over alkaline pH compared to acidic pH where the dye adsorption was low.

The observed pH effect on the MB adsorption with PANI can be discussed in terms of the chemical modification of its surface structure (Figure 9) and dye molecule when changing the solution pH. Some authors [70, 71] have shown that Emeraldine Salt starts losing rapidly its protons (H^+) when the solution pH approaches 3, and around pH 6–7, the polymer is entirely deprotonated leading to the generation of the leucoemeraldine base structure. These results were supported by Wang et al. [72] and Cabuk et al. [73], who found that the isoelectric points (pH_{IE}) of PANI, were ~5.8. and 6.1, respectively. The pH_{IE} is the pH at which the surface of a specific particle carries no net electrical charge. Therefore, a further increase in solution pH caused the polymer surface to be negatively charged, thus favoring the attractive electrostatic interactions with the cationic dye molecule at pH > pH_{IE}.

Moreover, the pH-chemical structure dependence of MB molecule has been extensively studied, and this dye was found to exhibit spectral changes related to the displacement of the maximum absorption wavelength even in the same pH range. MB is a weak base with a pK_a value of 3.8 and provides, in general, an almost neutral pH solution of ~6.8. Holmes and Snyder [73] have shown that MB was also stable at room temperature below pH 9.5. However, MB oxidation and/or demethylation began at pH > 9.5–9.8 and exhibited a slow increase in both rate and extent until pH 11. Beyond this value, rapid changes in the chemical structure took place, and the substances produced in highly alkaline solutions displayed metachromatic properties. Several authors [74–76] mentioned that these substances corresponded to methylene violet and methylene azure (A, B, C), causing a red or blue shift of the maximum absorbance; see Table 3.

In the case of acidic conditions and pH < 3.8, MB may undergo several structural modifications, mainly protonation and aggregation of MB monomers [77, 78]. The protonation can occur on both NMe_2 groups or at the central nitrogen atom of MB with a greater protonation tendency at the central nitrogen [79]. Therefore, MB is susceptible to generating neutral and charged chemical structures at low pH.

3.3.2. Kinetics and Equilibrium of MB Adsorption on PANI-EB. As stated in the previous section, MB adsorption on PANI at alkaline pH was higher than that obtained at acidic pH. For that reason, experimental kinetic and equilibrium studies of MB adsorption were carried out at pH 8 where the dye structure was also stable. MB adsorption kinetics on PANI-EB are reported in Figure 10. MB removal of PANI-EB improved with the contact time and dye concentration. Such observation could be attributed to the improvement of the driving forces needed to overcome the mass transfer limitations of dye molecules between the solid and aqueous phases [80]. Kinetic data revealed a fast dye removal during the first 15 min, after which the adsorption rate gradually decreased, and the equilibrium plateau was almost reached after 45 min. In general, the sharp increase of adsorption capacity at the beginning of the removal process could be assigned to the external surface available on PANI. MB removal of PANI-EB ranged from 62 to 81% for these initial concentrations. This MB removal by PANI could be associated with the interactions between the negatively charged surface of the adsorbent and the positively charged dye molecule.

The parameters for MB adsorption kinetics on PANI-EB were calculated with the pseudo-first-order model of Lagergren [81] and the pseudo-second-order model of Ho and McKay [82]. Results of data correlation and the corresponding model parameters are given in Table 4. Overall, a satisfactory correlation of experimental kinetic data was obtained with the pseudo-first-order model, in contrast to the pseudo-second-order model. Determination coefficients
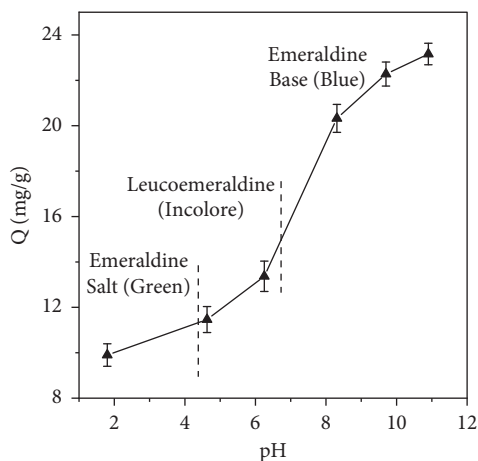
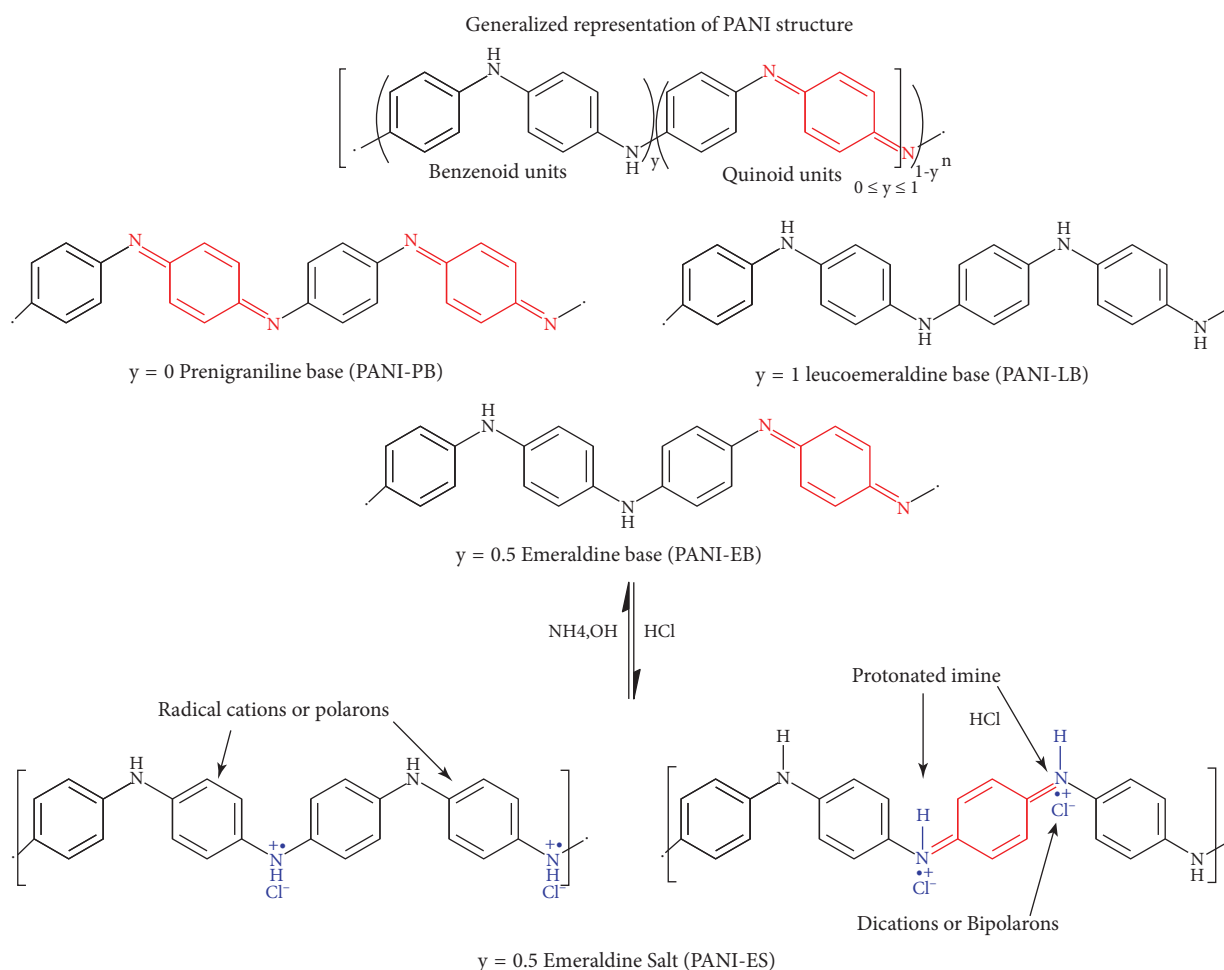FIGURE 8: Effect of the solution pH on the MB adsorption capacity of PANI.

FIGURE 9: Chemical structures of polyanilines.

(R^2) of this kinetic model were higher >0.9, and the calculated adsorption capacities were very close to those obtained during the experiments. These results were consistent with other studies related to MB adsorption onto PANI hydrogel [83] or the removal of other dyes using PANI nanoparticles [84]. MB adsorption rates ranged from 0.014 to 0.249 min^{-1} at 30 °C and pH 8.

Experimental data were also used to analyze other kinetic parameters associated with the mechanism by which MB molecule adsorbed on the PANI surface. For that, the intra-particle diffusion, Boyd, and Elovich models were employed. These models can be also used to identify the controlling steps of the adsorption process. The fitting results and the kinetic parameters are displayed, respectively, in Figure 11 and Table 5.

TABLE 3: Structures of methylene azure (*A*, *B*, *C*) and methylene violet [76].

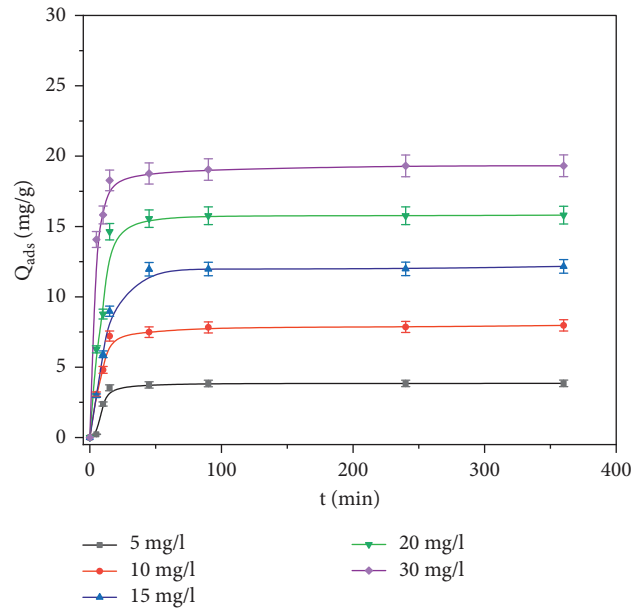| Name	Structure	λ_{max} (nm)
Methylene azure A		628
Methylene azure B		645
Methylene azure C		615
Methylene violet		610

FIGURE 10: Effect of initial concentration and contact time on MB removal and adsorption capacity of PANI-EB at 30°C and pH 8.

TABLE 4: Kinetic parameters for the MB adsorption on PANI-EB at pH 8 and 30°C.

		C_0 (mg/L)				
	$Q_{e\,(exp)}$ (mg/g)	5	10	15	20	30
		4.3	7.9	10.9	15.6	19.3
Pseudo-first order	$Q_{e\,(cal)}$ (mg/g)	4.7	7.8	11.0	15.7	18.8
	K_1 (min^{-1})	0.014	0.103	0.072	0.098	0.249
	R^2	0.58	0.94	0.94	0.92	0.88
	RMSE	1.67	0.50	0.84	1.22	0.78
Pseudo-second order	$Q_{e\,(cal)}$ (mg/g)	6.3	8.4	12.1	16.9	19.6
	K_2 (g/mg min)	0.002	0.016	0.007	0.008	0.026
	R^2	0.53	0.86	0.85	0.84	0.95
	RMSE	1.78	0.79	1.41	1.79	0.50

Figure 11(a) shows the dye adsorption capacity (Q_t) versus $t^{1/2}$. Two linear segments were identified for each initial dye concentration indicating that MB adsorption on PANI particles involved different mass transfer mechanisms. Furthermore, the model parameters suggested that the rate-controlling step in the adsorption of MB on PANI was not controlled by the intraparticle diffusion; but other mass transfer phenomena occurring at the boundary layer could also govern this separation process. Table 5 indicates smaller values of K_{d2} compared to K_{d1} for all initial concentrations, which could be attributed to the reduction of the free canals available for diffusion. Figure 11(b) displays Boyd model plots representing B_t as a function of time (t) with $B_t = -0.497 - \ln(1 - (q_t/q_e))$. This fitting provided linear

curves but none of them passed through the origin, thus indicating that the MB dye adsorption onto PANI-EB was controlled by film diffusion.

The experimental data were plotted using the Elovich model (Figure 11(c)) and the calculated parameters, α and β, are reported in Table 5. These parameters corresponded to the initial adsorption rate constant and the desorption constant, respectively. The determination coefficients (R^2) of various plots were somewhat far from the unity except for the highest concentration (30 mg/L). The tendency observed for the variation of α and β values (i.e., a decrease of β and an increase of α) can be associated with an enhancement of the adsorption rate [85]. These results could indicate that the MB@PANI-EB adsorption rate was concentration-
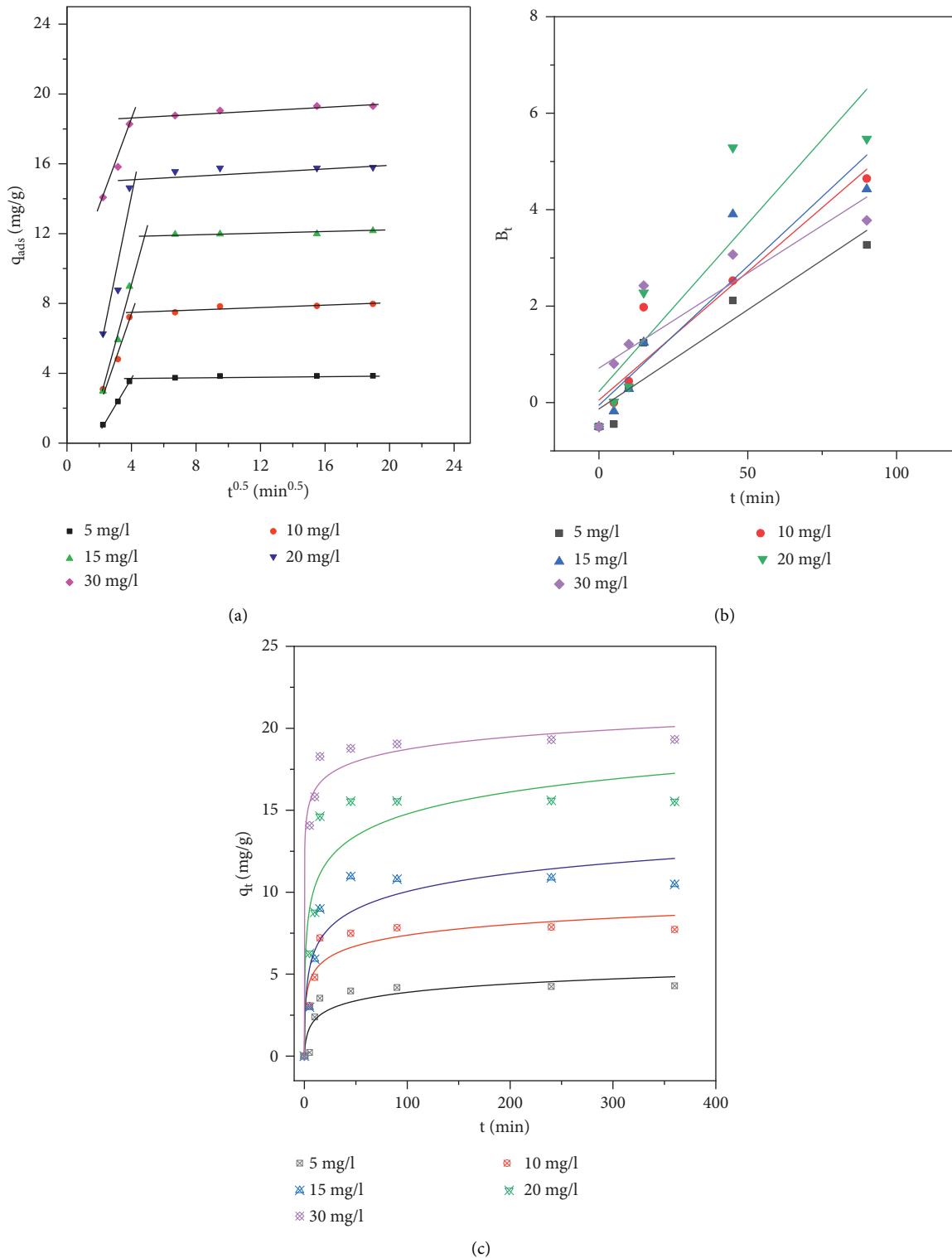
(a)

(b)

(c)

Figure 11: (a) Intraparticle diffusion model, (b) Boyd model, and (c) Elovich model for the MB adsorption on PANI.

dependent. An improvement in the MB adsorption rate with PANI-EB was observed when the dye amount increased.

Figure 12 reports the MB adsorption isotherm at pH 8 and 30 °C using PANI-EB and its correlation with various isotherm models, namely, Langmuir, Freundlich, Temkin,

D-R, and statistical physics models, summarized in Table 6. Overall, all the isotherm models showed high values of determination coefficients ($R^2 > 0.97$) and low values of RMSE. The statistical physics model was used to analyze the steric parameters associated with MB adsorption on PANI-

TABLE 5: Kinetic parameters of intraparticle diffusion, Boyd, and Elovich models for the MB@PANI-EB adsorption.

| Initial concentration	C_0 (mg/L)	5	10	15	20	30
		First linear section				
	C_1 (mg/g)	2.351	2.662	5.293	5.532	8.229
	K_{d1}(mg·g·min$^{1/2}$)	1.512	2.491	3.641	4.990	2.533
	R^2	0.998	0.975	0.992	0.951	0.978
Intraparticle diffusion	RMSE	0.059	0.497	0.372	0.812	0.514
		Second linear section				
	C_2 (mg/g)	3.727	7.381	11.842	15.516	18.558
	K_{d2}(mg·g·min$^{1/2}$)	0.007	0.032	0.014	0.016	0.044
	R^2	0.958	0.974	0.968	0.964	0.988
	RMSE	0.859	0.491	0.672	0.681	0.414
Boyd	R^2	0.864	0.883	0.836	0.757	0.669
	RMSE	0.553	0.659	0.863	1.319	0.911
	α (mg/g·min)	1.367	23.069	48.066	73.631	257.913
Elovich	β (g/mg)	1.341	1.057	0.635	0.517	0.925
	R^2	0.777	0.864	0.831	0.845	0.975
	RMSE	0.553	0.659	0.863	1.319	0.911

(a)

(b)
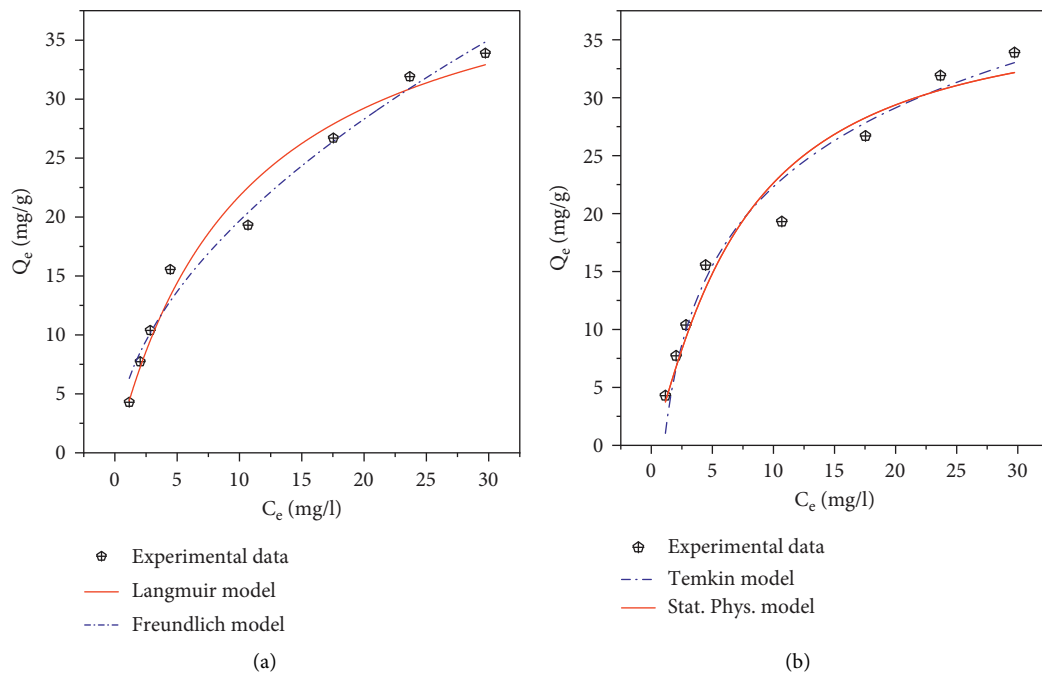
FIGURE 12: Continued.

(c)
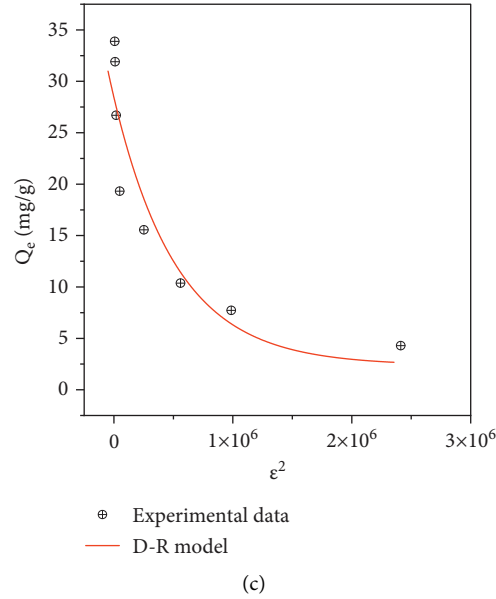
FIGURE 12: Isotherm of MB adsorption on PANI-EB, at pH 8 and 30°C, and its correlation with (a) Langmuir and Freundlich, (b) Temkin and statistical physics monolayer, and (c) Dubinin-Radushkevich models.

TABLE 6: Parameters of isotherm models for the MB adsorption on PANI-EB powder at pH 8 and 30°C.

Isotherm model	Equation			R^2	RMSE
Langmuir	$Q_e = (Q_m * K_L * C_e/1 + K_L * C_e)$	Q_{max} (mg/g) 44.41	K_L (L/mg) 0.096	0.978	1.81
Freundlich	$Q_e = K_F C_e^{1/n_F}$	K_F ((mg/g) $*$ (L/mg)$^{1/n}$) 4.62	n_F (L/mg) 1.48	0.983	1.59
Temkin	$Q_e = (RT/B_T) Ln (K_T * C_e)$	B_T (J/mol) 273.52	K_T (L/g) 1.18	0.974	1.94
Dubinin-Radushkevich	$Q_e = Q_{max} e^{-\beta \varepsilon}$	Q_{max} (mg/g) 34.21	E (kJ/mol) 0.888	0.973	1.83
Statistical physics—monolayer	$Q_e = (n D_m/1 + (C_{1/2}/C_2)^n)$	Q_{max} (mg/g) 40.17	n 1.2	0.995	0.49

EB. Note that this model showed the highest determination coefficient ($R^2 > 0.99$).

The monolayer model based on statistical physics theory provided a complementary description of the MB dye adsorption mechanism. This model was applied to the MB experimental adsorption data to sketch the dye adsorption orientation on the PANI-EB surface and to estimate the energy of dye-adsorbent interactions. Data fitting results showed that the parameter n, which described the number of MB dye molecule adsorbed per adsorption site, was greater than one (i.e., $n = 1.2$). Therefore, it can be concluded that more than one MB molecule interacted with the adsorption site on the PANI backbone. Additionally, this parameter suggested the formation of MB dimers in the aqueous solution. The adsorption orientation of MB molecules on the PANI-EB surface could be expected to be inclined during the dye removal, which was consistent with the computational chemistry results.

According to this statistical physics model, the energy for the MB-PANI-EB surface interaction can be estimated via the following expression:

$$\Delta E = R \cdot T \cdot \ln\left(\frac{C_s}{C_{1/2}}\right), \tag{5}$$

where C_s is the water solubility of MB dye (mg/L), $C_{1/2}$ is the estimated concentration at half-saturation (mg/L), and T is the adsorption temperature in K. The calculated adsorption energy was 14.0 kJ/mol and clearly indicated that only physical interactions were involved in the MB dye adsorption mechanism. However, it is convenient to remark that this value was lower than those obtained by AIMD calculations due to the absence of explicit water in the molecular simulations. The estimation of the saturation MB adsorption capacity (Q_{max}) of PANI-EB was 40.2 mg/g under alkaline conditions. This adsorption capacity of PANI-EB was superior to the values reported for other adsorbents at neutral pH [13, 14, 26, 83, 86–92]; see Table 7. It is necessary to remark that the removal performance of PANI-EB was lower than the adsorption capacities reported for PANI hydrogel (71.2 mg/g) [83] or PANI treated with polyacid (466.5 mg/g) [86] even at neutral pH. Therefore, the

TABLE 7: Maximum MB adsorption capacities reported for various PANI-based adsorbents and other materials.

Adsorbent	Maximum adsorption capacity (mg/g)	pH	T (°C)	References
PANI-EB	40.2	8–9	30	This study
PANI powder	11.8	6–7	30	[26]
PANI powder	11.2	6–7	25	[86]
PANI cross-linked	13.8	6–7	25	[87]
PANI nanoparticles	6.1	6–7	25	[14]
PANI nanotubes	9.2	6–7	25	[13]
Polyaniline hydrogel	71.2	6–7	25	[83]
Polyacid doped polyaniline	466.5	6–7	25	[86]
Phytic acid-doped PANI	43	6–7	35	[88]
PANI graphene oxide composites	14.2	6–7	25	[89]
PANI/reduced graphene oxide composites	19.2	6–7	25	[89]
PVDF/boron nitride nanosheets-based membranes	142.8	6.5	25	[92]
Flyash/TiO_2 modified chitosan biopolymer composite	35.1	7	25	[85]
Recycled PVDF beads	27.9	7	25	[93]
Boron nitride nanosheets	208.3	12	25	[94]

preparation of PANI composites and other derived materials is the best alternative to exploit the chemical and mechanical properties of this conductive polymer for the preparation of adsorbents in water treatment.

4. Conclusions

Theoretical computational chemistry calculations were performed to elucidate and explain the mechanism and intermolecular interactions for MB adsorption on doped and undoped PANI. Results showed that the adsorption energy of this dye on PANI-ES was slightly lower than that of PANI-EB where gas phase static DFT calculations estimated adsorption energies of −9.92 and −8.45 kJ/mol for MB@PANI-EB and MB@PANI-ES, respectively. Experimental and calculated infrared spectra of the MB-PANI systems and molecular dynamic simulations allowed us to conclude the relevant role of $\pi - \pi$ stacking and van der Waals interactions where a parallel adsorption position on the PANI surface could be expected. DFT calculations indicated that the PANI-EB surface showed the best adsorption properties for dye removal. These theoretical results were validated with experimental adsorption studies under different conditions of initial dye concentration, contact time, and initial pH. Experimental studies showed that MB adsorption on the PANI surface was significantly pH-dependent, thus confirming the theoretical results where the highest adsorption capacities were obtained at alkali solutions. Dye adsorption on PANI-EB was rapid within the first 10 min and the equilibrium was reached at about 100 min. Statistical physics calculation also sketched an inclined adsorption orientation of MB molecules on the PANI-EB surface, and a saturation adsorption capacity of 40.2 mg/g was estimated. The pseudo-second-order model and the intraparticle diffusion model were more suitable to fit adsorption data. The intraparticle diffusion and liquid-film diffusion processes were expected to control the adsorption rate of MB on PANI-EB. These theoretical and experimental results represent a full rationalization of MB@PANI adsorption behavior, which is fundamental to preparing new and advanced PANI materials for water detoxification.

Data Availability

The data used to support the findings of the study can be obtained from the corresponding author upon request.

Conflicts of Interest

The authors declared no potential conflicts of interest with respect to the research, authorship, and/or publication of this article.

Authors' Contributions

S. Djellali contributed to conceptualization, methodology, reviewing and editing of the manuscript, and supervision; A. Touati and M. Kebaili, investigation and original draft preparation. A. Semmeq conducted the simulation research, original draft preparation, and visualization; A. Bonilla-Petriciolet, methodology and reviewing and editing of the manuscript; M. Badawi, software, supervision, and reviewing and editing of the manuscript.

Acknowledgments

References

[1] M. Wan, "Some issues related to polyaniline micro-/nano-structures," *Macromolecular Rapid Communications*, vol. 30, pp. 963–975, 2009.

[2] Q. Hu, H. Liu, Z. Zhang, and Y. Xie, "Nitrate removal from aqueous solution using polyaniline modified activated carbon: optimization and characterization," *Journal of Molecular Liquids*, vol. 309, Article ID 113057, 2020.

[3] T. Vimal, K. Agrahari, R. K. Sonker, and R. Manohar, "Investigation of thermodynamical, dielectric and electro-optical

parameters of nematic liquid crystal doped with polyaniline and silver nanoparticles," *Journal of Molecular Liquids*, vol. 290, Article ID 111241, 2019.

[4] K. Aziz, F. Aziz, R. Mamouni, L. Aziz, and N. Saffaj, "Engineering of highly brachychiton populneus shells@polyaniline bio-sorbent for efficient removal of pesticides from wastewater: optimization using BBD-RSM approach," *Journal of Molecular Liquids*, vol. 346, Article ID 117092, 2022.

[5] A. Samadi, M. Xie, J. Li, H. Shon, C. Zheng, and S. Zhao, "Polyaniline-based adsorbents for aqueous pollutants removal: a review," *Chemical Engineering Journal*, vol. 418, Article ID 129425, 2021.

[6] X. Zhou, M. Xu, L. Wang, and X. Liu, "The adsorption of methylene blue by an amphiphilic block co-poly (arylene ether nitrile) microsphere-based adsorbent: kinetic, isotherm, thermodynamic and mechanistic studies," *Nanomaterials*, vol. 9, no. 10, p. 1356, 2019.

[7] P. A. Alaba, N. A. Oladoja, Y. M. Sani et al., "Insight into wastewater decontamination using polymeric adsorbents," *Journal of Environmental Chemical Engineering*, vol. 6, no. 2, pp. 1651–1672, 2018.

[8] M. Jouyandeh, S. M. R. Paran, M. Shabanian et al., "Curing behavior of epoxy/Fe_3O_4 nanocomposites: a comparison between the effects of bare Fe_3O_4, Fe_3O_4/SiO_2/chitosan and Fe_3O_4/SiO_2/chitosan/imide/phenylalanine-modified nanofillers," *Progress in Organic Coatings*, vol. 123, pp. 10–19, 2018.

[9] D. K. Yoo, H. J. An, N. A. Khan, G. T. Hwang, and S. H. Jhung, "Record-high adsorption capacities of polyaniline-derived porous carbons for the removal of personal care products from water," *Chemical Engineering Journal*, vol. 352, pp. 71–78, 2018.

[10] T. Luo, H. Liang, D. Chen, Y. Ma, and W. Yang, "Highly enhanced adsorption of methyl blue on weakly cross-linked ammonium-functionalized hollow polymer particles," *Applied Surface Science*, vol. 505, Article ID 144607, 2020.

[11] A. Alipour and M. Mansour Lakouarj, "Photocatalytic degradation of RB dye by CdS-decorated nanocomposites based on polyaniline and hydrolyzed pectin: isotherm and kinetic," *Journal of Environmental Chemical Engineering*, vol. 7, no. 1, Article ID 102837, 2019.

[12] P. Ahuja, S. K. Ujjain, I. Arora, and M. Samim, "Hierarchically grown NiO-decorated polyaniline-reduced graphene oxide composite for ultrafast sunlight-driven photocatalysis," *ACS Omega*, vol. 3, no. 7, pp. 7846–7855, 2018.

[13] M. M. Ayad and A. A. El-Nasr, "Adsorption of cationic dye (methylene blue) from water using polyaniline nanotubes base," *Journal of Physical Chemistry C*, vol. 114, no. 34, pp. 14377–14383, 2010.

[14] M. Ayad, G. El-Hefnawy, and S. Zaghlol, "Facile synthesis of polyaniline nanoparticles; its adsorption behavior," *Chemical Engineering Journal*, vol. 217, pp. 460–465, 2013.

[15] D. Mahanta, G. Madras, S. Radhakrishnan, and S. Patil, "Adsorption of sulfonated dyes by polyaniline emeraldine salt and its kinetics," *Journal of Physical Chemistry B*, vol. 112, no. 33, pp. 10153–10157, 2008.

[16] A. Taghizadeh, M. Taghizadeh, M. Jouyandeh et al., "Conductive polymers in water treatment: a review," *Journal of Molecular Liquids*, vol. 312, Article ID 113447, 2020.

[17] J. Huang, S. Virji, B. H. Weiller, and R. B. Kaner, "Polyaniline nanofibers: facile synthesis and chemical sensors," *Journal of the American Chemical Society*, vol. 125, no. 2, pp. 314-315, 2003.

[18] A. Bhattacharya and A. De, "Conducting composites of polypyrrole and polyaniline a review," *Progress in Solid State Chemistry*, vol. 24, no. 3, pp. 141–181, 1996.

[19] G. M. do Nascimento and N. A. Pradie, "Deprotonation, Raman dispersion and thermal behavior of polyaniline–montmorillonite nanocomposites," *Synthetic Metals*, vol. 217, pp. 109–116, 2016.

[20] J. Y. Shimano and A. G. MacDiarmid, "Polyaniline, a dynamic block copolymer: key to attaining its intrinsic conductivity?" *Synthetic Metals*, vol. 123, no. 2, pp. 251–262, 2001.

[21] L. Ai, J. Jiang, and R. Zhang, "Uniform polyaniline microspheres: a novel adsorbent for dye removal from aqueous solution," *Synthetic Metals*, vol. 160, no. 7-8, pp. 762–767, 2010.

[22] V. Janaki, B.-T. Oh, K. Shanthi, K.-J. Lee, A. K. Ramasamy, and S. Kamala-Kannan, "Polyaniline/chitosan composite: an eco-friendly polymer for enhanced removal of dyes from aqueous solution," *Synthetic Metals*, vol. 162, no. 11-12, pp. 974–980, 2012.

[23] P. Gharbani, "Synthesis of polyaniline-tin (II)molybdophosphate nanocomposite and application of it in the removal of dyes from aqueous solutions," *Journal of Molecular Liquids*, vol. 242, pp. 229–234, 2017.

[24] D. Mahanta, G. Madras, S. Radhakrishnan, and S. Patil, "Adsorption and desorption kinetics of anionic dyes on doped polyaniline," *Journal of Physical Chemistry B*, vol. 113, no. 8, pp. 2293–2299, 2009.

[25] Y. Xia, T. Li, J. Chen, and C. Cai, "Polyaniline (skin)/polyamide 6 (core) composite fiber: preparation, characterization and application as a dye adsorbent," *Synthetic Metals*, vol. 175, pp. 163–169, 2013.

[26] A.-N. Chowdhury, S. R. Jesmeen, and M. M. Hossain, "Removal of dyes from water by conducting polymeric adsorbent," *Polymers for Advanced Technologies*, vol. 15, no. 11, pp. 633–638, 2004.

[27] M. Bhaumik, R. I. McCrindle, A. Maity, S. Agarwal, and V. K. Gupta, "Polyaniline nanofibers as highly effective reuseable adsorbent for removal of reactive black 5 from aqueous solutions," *Journal of Colloid and Interface Science*, vol. 466, pp. 442–451, 2016.

[28] M. Bhaumik, R. McCrindle, and A. Maity, "Efficient removal of Congo red from aqueous solutions by adsorption onto interconnected polypyrrole-polyaniline nanofibres," *Chemical Engineering Journal*, vol. 228, pp. 506–515, 2013.

[29] S. Kalotra and R. Mehta, "Synthesis of polyaniline/clay nanocomposites by in situ polymerization and its application for the removal of acid green 25 dye from wastewater," *Polymer Bulletin*, vol. 78, no. 5, pp. 2439–2463, 2021.

[30] N. A. Gengec, M. Isgoren, M. Kobya, S. Veli, and E. Gengec, "Optimization of beidellite/polyaniline production conditions by central composite design for removal of acid yellow 194," *Journal of Polymers and the Environment*, vol. 26, no. 6, pp. 2619–2631, 2018.

[31] A. A. Babaei, A. Khataee, E. Ahmadpour, M. Sheydaei, B. Kakavandi, and Z. Alaee, "Optimization of cationic dye adsorption on activated spent tea: equilibrium, kinetics, thermodynamic and artificial neural network modeling," *Korean Journal of Chemical Engineering*, vol. 33, no. 4, pp. 1352–1361, 2016.

[32] M. Kermani, H. Izanloo, R. R. Kalantary, H. Salehi Barzaki, and B. Kakavandi, "Study of the performances of low-cost adsorbents extracted from rosa damascena in aqueous solutions decolorization," *Desalination and Water Treatment*, vol. 80, pp. 357–369, 2017.

[33] S. Maeda and S. P. Armes, "Surface area measurements on conducting polymer-inorganic oxide nanocomposites," *Synthetic Metals*, vol. 73, no. 2, pp. 151–155, 1995.

[34] T. Yao, S. Guo, C. Zeng, C. Wang, and L. Zhang, "Investigation on efficient adsorption of cationic dyes on porous magnetic polyacrylamide microspheres," *Journal of Hazardous Materials*, vol. 292, pp. 90–97, 2015.

[35] D. Li, Y. Yang, C. Li, and Y. Liu, "A mechanistic study on decontamination of methyl orange dyes from aqueous phase by mesoporous pulp waste and polyaniline," *Environmental Research*, vol. 154, pp. 139–144, 2017.

[36] A. Yadav, S. S. Dindorkar, S. B. Ramisetti, and N. Sinha, "Simultaneous adsorption of methylene blue and arsenic on graphene, boron nitride and boron carbon nitride nanosheets: insights from molecular simulations," *Journal of Water Process Engineering*, vol. 46, Article ID 102653, 2022.

[37] T. K. Mahto, S. Chandra, C. Haldar, and S. K. Sahu, "Kinetic and thermodynamic study of polyaniline functionalized magnetic mesoporous silica for magnetic field guided dye adsorption," *RSC Advances*, vol. 5, no. 59, pp. 47909–47919, 2015.

[38] E. N. Zare, A. Motahari, and M. Sillanpää, "Nanoadsorbents based on conducting polymer nanocomposites with main focus on polyaniline and its derivatives for removal of heavy metal ions/dyes: a review," *Environmental Research*, vol. 162, pp. 173–195, 2018.

[39] B. Lellis, C. Z. Fávaro-Polonio, J. A. Pamphile, and J. C. Polonio, "Effects of textile dyes on health and the environment and bioremediation potential of living organisms," *Biotechnology Research and Innovation*, vol. 3, no. 2, pp. 275–290, 2019.

[40] J. P. Perdew, K. Burke, and M. Ernzerhof, "Generalized gradient approximation made simple," *Physical Review Letters*, vol. 77, no. 18, pp. 3865–3868, 1996.

[41] M. Frisch, G. W. Trucks, H. B. Schlegel et al., *Gaussian 09*, Gaussian, Inc, Wallingford, CT, USA, 2009.

[42] V. Barone and M. Cossi, "Quantum calculation of molecular energies and energy gradients in solution by a conductor solvent model," *The Journal of Physical Chemistry A*, vol. 102, no. 11, pp. 1995–2001, 1998.

[43] M. Cossi, N. Rega, G. Scalmani, and V. Barone, "Energies, structures, and electronic properties of molecules in solution with the C-PCM solvation model," *Journal of Computational Chemistry*, vol. 24, no. 6, pp. 669–681, 2003.

[44] J. VandeVondele, M. Krack, F. Mohamed, M. Parrinello, T. Chassaing, and J. Hutter, "Quickstep: fast and accurate density functional calculations using a mixed Gaussian and plane waves approach," *Computer Physics Communications*, vol. 167, no. 2, pp. 103–128, 2005.

[45] A. K. Mishra, "DFT study of structural, vibrational and electronic properties of polyaniline pernigraniline model compounds," *Journal of Computational Science*, vol. 10, pp. 195–208, 2015.

[46] S. Grimme, "Semiempirical GGA-type density functional constructed with a long-range dispersion correction," *Journal of Computational Chemistry*, vol. 27, no. 15, pp. 1787–1799, 2006.

[47] S. Goedecker, M. Teter, and J. Hutter, "Separable dual-space Gaussian pseudopotentials," *Physical Review B: Condensed Matter*, vol. 54, no. 3, pp. 1703–1710, 1996.

[48] J. VandeVondele and J. Hutter, "Gaussian basis sets for accurate calculations on molecular systems in gas and condensed phases," *The Journal of Chemical Physics*, vol. 127, no. 11, Article ID 114105, 2007.

[49] G. Lippert, J. Hutter, and M Parrinello, "A hybrid Gaussian and plane wave density functional scheme," *Molecular Physics*, vol. 92, no. 3, pp. 477–487, 1997.

[50] M. Ceriotti, G. Bussi, and M. Parrinello, "Langevin equation with colored noise for constant-temperature molecular dynamics simulations," *Physical Review Letters*, vol. 102, no. 2, Article ID 020601, 2009.

[51] "GLE4MD Project: Automatic Input Generation," 2020, https://gle4md.org/index.html?page=matrix.

[52] J. Stejskal and R. G. Gilbert, "Polyaniline. Preparation of a conducting polymer (IUPAC technical report)," *Pure and Applied Chemistry*, vol. 74, no. 5, pp. 857–867, 2002.

[53] A. Mittal, A. Malviya, D. Kaur, J. Mittal, and L. Kurup, "Studies on the adsorption kinetics and isotherms for the removal and recovery of methyl orange from wastewaters using waste materials," *Journal of Hazardous Materials*, vol. 148, no. 1-2, pp. 229–240, 2007.

[54] B. J. Barner and R. M. Corn, "Electrochemical and vibrational spectroscopic studies of coadsorption: the formation of mixed monolayers of methylene blue and long-chain dithioethers at sulfur-modified polycrystalline gold surfaces," *Langmuir*, vol. 6, no. 5, pp. 1023–1030, 1990.

[55] O. V. Ovchinnikov, A. V. Evtukhova, T. S. Kondratenko, M. S. Smirnov, V. Yu. Khokhlov, and O. V. Erina, "Manifestation of intermolecular interactions in FTIR spectra of methylene blue molecules," *Vibrational Spectroscopy*, vol. 86, pp. 181–189, 2016.

[56] X.-R. Zeng and T.-M. Ko, "Structures and properties of chemically reduced polyanilines," *Polymer*, vol. 39, no. 5, pp. 1187–1195, 1998.

[57] J. Tang, X. Jing, B. Wang, and F. Wang, "Infrared spectra of soluble polyaniline," *Synthetic Metals*, vol. 24, no. 3, pp. 231–238, 1988.

[58] Y. Cao, S. Li, Z. Xue, and D. Guo, "Spectroscopic and electrical characterization of some aniline oligomers and polyaniline," *Synthetic Metals*, vol. 16, no. 3, pp. 305–315, 1986.

[59] Y. H. Kim, C. Foster, J. Chiang, and A. J. Heeger, "Photoinduced localized charged excitations in polyaniline," *Synthetic Metals*, vol. 26, no. 1, pp. 49–59, 1988.

[60] J. Tanaka, N. Mashita, K. Mizoguchi, and K. Kume, "Molecular and electronic structures of doped polyaniline," *Synthetic Metals*, vol. 29, no. 1, pp. 175–184, 1989.

[61] E. Kang, "Polyaniline: a polymer with many interesting intrinsic redox states," *Progress in Polymer Science*, vol. 23, no. 2, pp. 277–324, 1998.

[62] J. P. Pouget, M. E. Jozefowicz, A. J. Epstein, X. Tang, and A. G. MacDiarmid, "X-ray structure of polyaniline," *Macromolecules*, vol. 24, no. 3, pp. 779–789, 1991.

[63] W. Łużny, M. Śniechowski, and J. Laska, "Structural properties of emeraldine base and the role of water contents: X-ray diffraction and computer modelling study," *Synthetic Metals*, vol. 126, no. 1, pp. 27–35, 2002.

[64] P. R. Somani, R. Marimuthu, A. K. Viswanath, and S. Radhakrishnan, "Thermal degradation properties of solid polymer electrolyte (poly (vinyl alcohol) + phosphoric acid)/ methylene blue composites," *Polymer Degradation and Stability*, vol. 79, no. 1, pp. 77–83, 2003.

[65] O. V. Ovchinnikov, S. V. Chernykh, M. S. Smirnov et al., "Analysis of interaction between the organic dye methylene blue and the surface of AgCl (I) microcrystals," *Journal of Applied Spectroscopy*, vol. 74, no. 6, pp. 809–816, 2007.

[66] D. S. Vicentini, R. V. Salvatierra, A. J. G. Zarbin, L. G. Dutra, and M. M. Sá, "Synthesis and characterization of carboxyl-substituted polyanilines doped with halogenated acids:

combining conductivity with solubility," *Journal of the Brazilian Chemical Society*, vol. 25, pp. 1939–1947, 2014.

[67] K. Zarrini, A. A. Rahimi, F. Alihosseini, and H. Fashandi, "Highly efficient dye adsorbent based on polyaniline-coated nylon-6 nanofibers," *Journal of Cleaner Production*, vol. 142, pp. 3645–3654, 2017.

[68] A.-N. Chowdhury, F. S. Saleh, M. R. Rahman, and A. Rahim, "Influence of pH on the specific surface area of polyaniline matrices," *Journal of Applied Polymer Science*, vol. 109, no. 3, pp. 1764–1771, 2008.

[69] N. Wang, J. Chen, J. Wang, J. Feng, and W. Yan, "Removal of methylene blue by Polyaniline/TiO$_2$ hydrate: adsorption kinetic, isotherm and mechanism studies," *Powder Technology*, vol. 347, pp. 93–102, 2019.

[70] J.-C. Chiang and A. G. MacDiarmid, ""Polyaniline": protonic acid doping of the emeraldine form to the metallic regime," *Synthetic Metals*, vol. 13, no. 1-3, pp. 193–205, 1986.

[71] W. S. Huang and A. G. MacDiarmid, "Optical properties of polyaniline," *Polymer*, vol. 34, no. 9, pp. 1833–1845, 1993.

[72] J. Wang, B. Deng, H. Chen, X. Wang, and J. Zheng, "Removal of aqueous Hg (II) by polyaniline: sorption characteristics and mechanisms," *Environmental Science and Technology*, vol. 43, no. 14, pp. 5223–5228, 2009.

[73] M. Cabuk, M. Yavuz, and H. I. Unal, "Electrokinetic properties of biodegradable conducting polyaniline-graft-chitosan copolymer in aqueous and non-aqueous media," *Colloids and Surfaces A: Physicochemical and Engineering Aspects*, vol. 460, pp. 494–501, 2014.

[74] W. C. Holmes and E. F. Snyder, "The atmospheric oxidation, or dealkylation, of aqueous solutions of methylene blue," *Stain Technology*, vol. 4, no. 1, pp. 7–10, 1929.

[75] W. J. MacNeal and J. A. Killian, "Chemical studies on polychrome methylene blue 1," *Journal of the American Chemical Society*, vol. 48, no. 3, pp. 740–747, 1926.

[76] G. S. Singhal and E. Rabinowitch, "Changes in the absorption spectrum of methylene blue with pH," *Journal of Physical Chemistry*, vol. 71, no. 10, pp. 3347–3349, 1967.

[77] A. Mills, D. Hazafy, J. Parkinson, T. Tuttle, and M. G. Hutchings, "Effect of alkali on methylene blue (C. I. basic blue 9) and other thiazine dyes," *Dyes and Pigments*, vol. 88, no. 2, pp. 149–155, 2011.

[78] M. G. Neumann, F. Gessner, C. C. Schmitt, and R. Sartori, "Influence of the layer charge and clay particle size on the interactions between the cationic dye methylene blue and clays in an aqueous suspension," *Journal of Colloid and Interface Science*, vol. 255, no. 2, pp. 254–259, 2002.

[79] E. K. Golz and D. A. Vander Griend, "Modeling methylene blue aggregation in acidic solution to the limits of factor Analysis," *Analytical Chemistry*, vol. 85, no. 2, pp. 1240–1246, 2013.

[80] K. Sarmah and S. Pratihar, "Synthesis, characterization, and photocatalytic application of iron oxalate capped Fe, Fe-Cu, Fe-Co, and Fe-Mn oxide nanomaterial," *ACS Sustainable Chemistry & Engineering*, vol. 5, no. 1, pp. 310–324, 2017.

[81] H. Brenner and L. G. Leal, "Interfacial resistance to interphase mass transfer in quiescent two-phase systems," *AIChE Journal*, vol. 24, no. 2, pp. 246–254, 1978.

[82] S. Lagergren, *About the Theory of So-Called Adsorption of Soluble Substances*, Royal Swedish Academy of Sciences, Stockholm, Sweden, 1898.

[83] Y. S. Ho and G. McKay, "Pseudo-second order model for sorption processes," *Process Biochemistry*, vol. 34, no. 5, pp. 451–465, 1999.

[84] B. Yan, Z. Chen, L. Cai, Z. Chen, J. Fu, and Q. Xu, "Fabrication of polyaniline hydrogel: synthesis, characterization and adsorption of methylene blue," *Applied Surface Science*, vol. 356, pp. 39–47, 2015.

[85] R. Gajera, R. V. Patel, A. Yadav, and P. K. Labhasetwar, "Adsorption of cationic and anionic dyes on photocatalytic flyash/TiO$_2$ modified chitosan biopolymer composite," *Journal of Water Process Engineering*, vol. 49, Article ID 102993, 2022.

[86] M. Saad, H. Tahir, J. Khan, U. Hameed, and A. Saud, "Synthesis of polyaniline nanoparticles and their application for the removal of crystal violet dye by ultrasonicated adsorption process based on response surface methodology," *Ultrasonics Sonochemistry*, vol. 34, pp. 600–608, 2017.

[87] S. H. Chien and W. R. Clayton, "Application of Elovich equation to the kinetics of phosphate release and sorption in soils," *Soil Science Society of America Journal*, vol. 44, no. 2, pp. 265–268, 1980.

[88] J. Shen, S. Shahid, I. Amura, A. Sarihan, M. Tian, and E. A. Emanuelsson, "Enhanced adsorption of cationic and anionic dyes from aqueous solutions by polyacid doped polyaniline," *Synthetic Metals*, vol. 245, pp. 151–159, 2018.

[89] M. Ayad and S. Zaghlol, "Nanostructured crosslinked polyaniline with high surface area: synthesis, characterization and adsorption for organic dye," *Chemical Engineering Journal*, vol. 204-206, pp. 79–86, 2012.

[90] M. Duhan and R. Kaur, "Phytic acid doped polyaniline nanofibers: an advanced adsorbent for methylene blue dye," *Environmental Nanotechnology, Monitoring & Management*, vol. 12, Article ID 100248, 2019.

[91] E. A. El-Sharkaway, R. M. Kamel, I. M. El-Sherbiny, and S. S. Gharib, "Removal of methylene blue from aqueous solutions using polyaniline/graphene oxide or polyaniline/reduced graphene oxide composites," *Environmental Technology*, vol. 41, no. 22, pp. 2854–2862, 2019.

[92] R. S. Bangari, A. Yadav, J. Bharadwaj, and N. Sinha, "Boron nitride nanosheets incorporated polyvinylidene fluoride mixed matrix membranes for removal of methylene blue from aqueous stream," *Journal of Environmental Chemical Engineering*, vol. 10, no. 1, Article ID 107052, 2022.

[93] R. V. Patel, G. B. Raj, S. Chaubey, and A. Yadav, "Investigation on the feasibility of recycled polyvinylidene difluoride polymer from used membranes for removal of methylene blue: experimental and DFT studies," *Water Science and Technology*, vol. 86, no. 1, pp. 194–210, 2022.

[94] R. S. Bangari, A. Yadav, P. Awasthi, and N. Sinha, "Experimental and theoretical analysis of simultaneous removal of methylene blue and tetracycline using boron nitride nanosheets as adsorbent," *Colloids and Surfaces A: Physicochemical and Engineering Aspects*, vol. 634, Article ID 127943, 2022.